JAMECH
Vol. 46, No. 1, January. 2015, pp 51- 62

Closed-form Molecular Mechanics Formulations for the 3D Local Buckling and 2D Effective Young's Modulus of the Nanosheets

Z. Sarvi [1], M. Shariyat [2*] and M. Asgari [3]

1. M.Sc., Faculty of Mechanical Engineering, K.N. Toosi University of Technology, Tehran, Iran

2. Professor, Faculty of Mechanical Engineering, K.N. Toosi University of Technology, Tehran, Iran

3. Assistant Professor, Faculty of Mechanical Engineering, K.N. Toosi University of Technology, Tehran, Iran

Received 16 January 2015; Accepted 7 February 2015

Abstract

A closed form three-dimensional solution is presented for determination of the local buckling (cell buckling) load of the nanosheets. Moreover, an expression is proposed for the effective 2D Young's modulus of the unit cell of the nanosheet. In this regard, a three-dimensional efficient space-frame-like geometrical model with angular and extensional compliances is considered to investigate stability and effective Young's modulus of the nanosheet in terms of the generally possible relative movements of the atoms of the unit cell, in the Cartesian coordinates. The molecular dynamics approach is employed in development of the formulation, taking into account the force constants and bond characteristics. The governing equations are derived based on the principle of minimum total potential energy. Results of the special cases of each of the proposed expressions are verified by the results available in literature or results of the traditional approaches. Comparisons are made with various buckling results reported for different nanosheets, based on different approaches of determination of the stiffness parameters, and a good agreement is noticed.

Keywords: *effective 2D Young's modulus, local buckling load, molecular mechanics, unit cell of a nanosheet.*

1. Introduction

A brief survey of the progress and evolution of the modern technologies reveals that the scale of the material structure which attracts the researchers' attention has changed significantly in the past decades. The main subjects of interest have been directed gradually toward the micro and finally, nano structures. The nanostructures may be categorized as zero-dimensional (0D) fullerenes, 1D such as nanowires and nanotubes, 2D allotropes such as graphene, and three-dimensional (3D) such as the nanocrystalline diamonds.

The first discovery of the nano-dimensional materials goes back to the discovery of the carbon nanotubes in 1976 [1] and the first computer simulations of this new nanostructure were performed almost 20 years later [2]. But the 2D form of the carbon nanostructure remained unknown until 2004, in which

* Corresponding author, Tel: 09122727199
E-mail: m_shariyat@yahoo.com , shariyat@kntu.ac.ir.

Novoselov et al. [3] produced a stable 2D carbon nanostructure that was called by them as graphene. After this discovery, the question arose among the researchers whether other 2D forms of the nano-materials exist or not. Thereafter, nanosheets were introduced to the scientific society. Other 2D nanostructures such as boron nitride (BN) were discovered after the graphene. In 2004, the first BN nanosheet was produced by Corso et al. [4]. Other studies have been performed in order to investigate characteristics of MoS_2 nanosheets, silicone, gramanene, layered group-IV and group-III metal chalcogenides, etc. [5, 6].

From the physical point of view, buckling under compressive loads is a phenomenon that may be expected to occur for any structure, regardless of the scale or form of the structure. It is evident that the buckling phenomenon affects the functionality of the nanostructures. This phenomenon has also been investigated for the various forms of the nanostructures through different methods and approaches. However, these works have usually focused on the nanotubes much more than the nanosheets, due to the earlier discovery of the nanotubes in comparison to the other forms of the nanostructures.

Numerous researchers used continuum mechanics approaches to propose closed- form expressions for determination of the effective mechanical properties and buckling loads of the nanotubes. They generally employed the nonlocal Timoshenko beam theory, considering the tubes as beams or shells in order to use the traditional beam or shell theories [7, 8]. Sudak [9] presented a column model for buckling of the multiwalled carbon nanotubes, using the nonlocal continuum mechanics. The resulting expression for the critical axial strain confirmed the significant contribution of the small scale effects to the mechanical behavior of the multiwalled carbon nanotubes. Wang and Wang [10] presented the constitutive relations of the nonlocal elasticity of the carbon nanotubes as Euler–Bernoulli or Timoshenko beams or cylindrical shells. Lu et al. [11] investigated vibration characteristics of the single- or multi-walled carbon nanotubes, based on a nonlocal beam model. Due to the similarities between the carbon nanotubes and nanorings, Shi et al. [12] presented an atomic-scale finite element vibration mode transformation analysis for both carbon nanorings and single-walled carbon nanotubes, considering the inertia terms.

Moosavi et al. [13] used a shear -deformable theory for free in- plane vibration analysis of the nanorings, based on the nonlocal elasticity theory. Danesh et al. [14] studied the small-scale effect on the axial vibrations of a tapered nanorod, employing the nonlocal elasticity theory. Similarly, Aydogdu [15] studied axial vibrations of a single -walled carbon nanotube embedded in an elastic medium, using the nonlocal elasticity theory. Arash and Wang [16] presented a literature survey on the recent studies on the application of the nonlocal continuum theory in modeling of carbon nanotubes and graphene sheets. They discussed the superiority of nonlocal continuum models over their local counterparts, the necessity of the calibration of the small-scale parameters, and the applicability of the nonlocal continuum models.

Determination of the effective material properties and buckling loads of the nanosheets has usually been accomplished through using the traditional plate theories and approaches which are adequate for the continuous structures. Pradhan [17] reformulated a high-order shear-deformation theory using the nonlocal differential constitutive relations of Eringen. After deriving the equations of motion of the nonlocal theories, he employed Navier's approach to study buckling of the nanoplates, such as the graphene sheets. Narender [18] studied buckling of the isotropic nanoplates, using a two variable refined plate theory and the nonlocal small-scale effects. He obtained a closed-form solution for determination of buckling load of a simply supported rectangular nanoplate subjected to an in-plane loading, based on Navier's method. Samaei et al. [19] investigated effects of the length scale on buckling behavior of a single-layer graphene sheet embedded in a Pasternak elastic medium through a nonlocal Mindlin plate theory.

Farajpour et al. [20] studied buckling behaviors of clamped and simply supported circular single-layered graphene sheets under uniform radial compression, considering the small-scale effects and using a nonlocal elasticity theory. Later, they investigated buckling response of an orthotropic single-layered graphene sheet, using a nonlocal

elasticity theory [21]. Narender and Gopalakrishnan [22] analyzed buckling of the orthotropic nanoplates such as graphene, using the two-variable plate theory and considering the nonlocal and small-scale effects. They obtained a closed-form solution for buckling of a simply supported rectangular orthotropic nanoplate, using Navier's method. Ansari et al. [23] studied buckling of the silicon carbide nanotubes through using 3D space frame finite elements. Samaei and Hashemi [24], proposed an analytical solution for buckling analysis of simply supported rectangular single-layered graphene sheets under in-plane loads using a nonlocal Mindlin plate theory. Ansari et al. [25] investigated buckling behavior of the single-layered silicon carbide nanosheets by employing an atomistic finite element model that preserved the discrete nature of the nanosheets.

Bedroud et al. [26] presented an analytical solution for the buckling analysis of moderately thick circular/annular Mindlin nanoplates under uniform radial compressive loads. In order to consider small-scale effects, they employed the nonlocal elasticity theory. Sobhy [27] proposed a Levy-type solution for bending response analysis of single-layered graphene sheets subjected to mechanical loads, in thermal environments. Hosseini-Hashemi et al. [28] presented analytical closed-form Levy-type solutions to include the small-scale effects in the buckling and the transverse vibration analyses of the rectangular nanoplates based on Reddy's nonlocal third-order shear-deformation plate theory.

In majority the aforementioned works (with exception of Refs. [23, 25]), the nanosheet was modeled as a continuous plate; so that the relevant closed-form expressions of the buckling of the nanosheet have been derived based on the traditional plate theories. However, as mentioned in [23, 25] this may lead to some errors in the results due to the discontinuity in the structure of the nanosheet. On the other hand, the buckling mechanism of the plates is quite different from that of the space frame-like structures. This difference can import some errors in the final formulations and results. Therefore, employing a space-frame structure whose members and joints are the bonds and atoms, respectively, leads to more accurate results.

In the present research, by modeling the nanosheet by a space frame-like structure, closed-form expressions are proposed for the local buckling and effective 2D Young modulus analyses of the nanosheet. The proposed procedure may be employed much easier than the common approaches used in the previous studies. While this simplicity is induded in the proposed model, effects of the discontinuity of the structure are also taken into account. On the other hand, none of the continuous plate theories have been derived based on the continuum mechanics approach; an issue that has also been taken into account in the present research to study and formulate characteristics of the considered special structure. In this regard, a unit cell that may be repeated in the whole structure, is adopted. Starting from the basic geometrical relations and employing concepts related to the buckling occurrence, a close-form expression is derived for the buckling load. Verification of the results is accomplished by comparing the Young moduli expressions of the present research with those available in the literature. Then, the buckling expression is verified by a conceptual example.

2. The Structural Modeling and Formulation

2.1. The potential energy expression of the nanostructure

From the molecular mechanics point of view, a nanostructure can be regarded as a large molecule consisting of some atoms. The atomic nuclei can be regarded as material points. Their motions are regulated by a force field which is generated by the electron-nucleus interactions and nucleus-nucleus interactions [29]. Usually, the force field may be expressed in the form of steric potential energy. It depends solely on the relative positions of the nuclei constituting the molecule. The potential energy of an arbitrary molecule geometry may be written as a superposition of various two-body, three-body, and four-body interactions. Therefore, the potential energy, E, may be expressed as a sum of energies associated with valence or bonded interactions and non-bonded interactions [30]:

$$E = \sum E_r + \sum E_\theta + \sum E_\phi + \sum E_\omega + \sum E_{vdw} + \sum E_{el} \qquad (1)$$

The valence interactions consist of bond stretching (E_r), bond angle bending (E_θ), dihedral angle torsion (E_ϕ), and inversion terms (E_ω). The nonbonded interactions consist of the van der Waals (E_{vdw}) and electrostatic (E_{el}) terms.

The harmonic approximation is adequate for description of the potential energy, based on the small deformations assumption. Merging the two terms of out-of-plane torsion and dihedral angle torsion in one term, based on the harmonic approximation, the following definitions may be presented for the energy terms of the interatomic interactions appeared in Equation [31]:

$$E_r = \frac{1}{2}k_r\left(r - r_0\right)^2 = \frac{1}{2}k_r\left(\Delta r\right)^2 \quad (2)$$

$$E_\theta = \frac{1}{2}k_\theta\left(\theta - \theta_0\right)^2 = \frac{1}{2}k_\theta\left(\Delta\theta\right)^2 \quad (3)$$

$$E_\tau = E_\phi + E_\omega = \frac{1}{2}k_\tau\left(\Delta\phi\right)^2 \quad (4)$$

where k_r, k_θ and k_τ are the bond stretching-force constant, bond angle-bending moment constant, and torsional resistance, respectively, and the symbols Δr, $\Delta\theta$, and $\Delta\phi$ represent the bond stretching increment, the in-plane bond angle change, and the out-of-plane angle change of the bond due to twisting, respectively.

In hexagonal nanostructures such as graphene and h-BN nanosheets, boron and nitrogen or carbon atoms are bonded to each other by covalent bonds to form a hexagonal network. When a nanosheet is subjected to external forces, displacements of the individual atoms are constrained by these bonds. Total deformation of the nanosheet is a result of the interactions of these bonds. By considering the covalent bonds as connecting elements between boron and nitrogen atoms, a nanosheet can be simulated as the space frame-like structure depicted in Figure 1, in which the atoms act as joints of the connected elements. Therefore, its behavior can be analyzed based on the classical structural mechanics approaches.

Le [32] derived a closed-form expression for predicting Young modulus in a nanosheet, considering a space-frame like structure. His approach takes into account just two terms of the total potential energy, while in general, for covalent systems, the main contributions to the total steric energy come from the first four terms, which are associated with four-body potentials. In order to extend this approach, we apply the third and fourth terms by considering 3-D deformations of the structure. As shown in Figure 1, a unit cell was selected which can be repeated through the whole structure. The Young modulus and buckling load are obtained based on this unit cell.

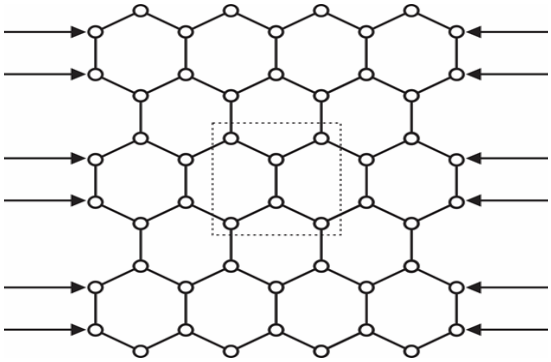

Fig. 1. Modeling the nanosheets by a space frame-like structure

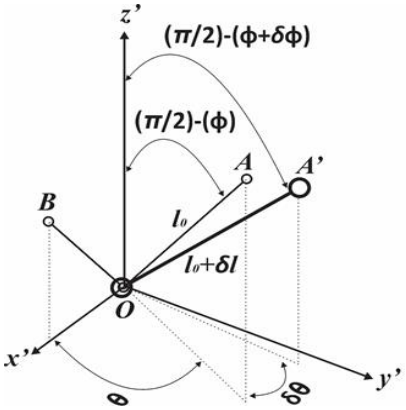

Fig. 2. Possible relative movements of the nanostructure

The possible relative deformations of the unit cell are shown in Figure 2. As it can be seen, the angle between the two elements shown in Figure 2 (i.e., OA and OB), θ, is one of the characteristics of the lattice and is equal to 120 degrees for the hexagonal lattices that constitute the graphene, BN nanosheet, etc. The spatial angle of the element with the xy-plane is denoted by ϕ and the initial length of the element is assumed to be l_0. Variations of θ, ϕ and l_0 are denoted by $\delta\theta$, $\delta\phi$ and δl, respectively. Therefore, the whole unit cell has six degrees of freedom.

The selected unit cell shown in Figure 3 is symmetric with respect to the y-axis. For this reason, relations are obtained for one half

(atoms number 2, 3, 4, 6) of the structure, for the sake of computational economy. The top view and the 3D illustration of the considered configuration (the undeformed configuration) are shown in Figures 3 and 4, respectively, along with the considered uniaxial compressive load that acts along the zigzag direction. It is assumed that nodes 1, 2, 5, and 6 can move in both x and y directions, while nodes 3 and 4, due to symmetry, have the opportunity to just move along z direction, as shown in Figure 3.

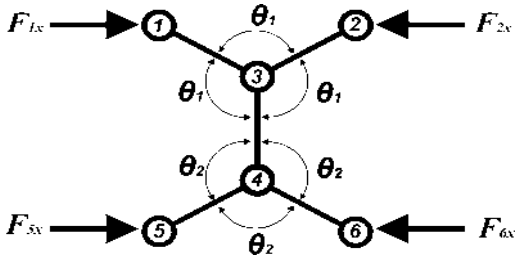

Fig. 3. The considered unit cell along with the applied compressive load

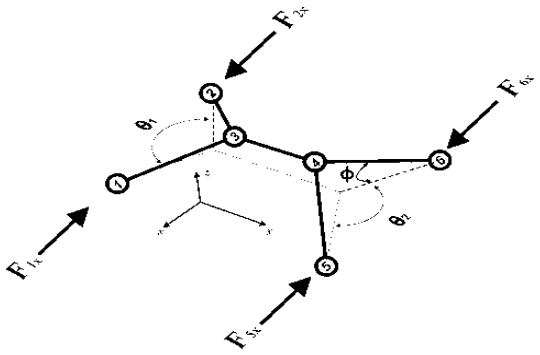

Fig. 4. Spatial configuration of the considered space frame structure

Therefore, the potential energy expression of the deformed unit cell may be rewritten as

$$E_{internal}=\frac{k_r}{2}\left[(\delta l_{13})^2+(\delta l_{23})^2+(\delta l_{46})^2+(\delta l_{45})^2\right]+\frac{k_\theta}{2}\left[(\delta\theta_{123})^2+(\delta\theta_{234})^2+(\delta\theta_{134})^2+(\delta\theta_{546})^2+(\delta\theta_{345})^2+(\delta\theta_{346})^2\right]+\frac{k_\tau}{2}\left[(\delta\phi_{13})^2+(\delta\phi_{23})^2+(\delta\phi_{45})^2+(\delta\phi_{46})^2\right] \quad (5)$$

where due to symmetry, one may set:

$$\delta l_{13}=\delta l_{23},\ \delta l_{45}=\delta l_{46}, \quad (6a)$$

$$\delta\theta_{123}=-2\delta\theta_1,\ \delta\theta_{134}=\delta\theta_1,\ \delta\theta_{234}=\delta\theta_1,\ \delta\theta_{546}=-2\delta\theta_2,\ \delta\theta_{345}=\delta\theta_2,\ \delta\theta_{346}=\delta\theta_2 \quad (6b)$$

$$\delta\phi_{13}=\delta\phi_{23},\ \delta\phi_{45}=\delta\phi_{46}, \quad (6c)$$

So, Equation (5) may be reduced to:

$$E_{internal}=k_r\left[(\delta l_{23})^2+(\delta l_{46})^2\right]+3k_\theta\left[(\delta\theta_1)^2+(\delta\theta_2)^2\right]+k_\tau\left[(\delta\phi_{23})^2+(\delta\phi_{46})^2\right] \quad (7)$$

The deformations may be expressed as functions of the relative atomic displacements. Starting from the geometry displayed in Figure 4, the final state of the deformation vector may be described in two forms. First it may be written in terms of the changed lengths using their projections on *x*, *y*, and *z* axes. Then, variations of initial length's projections along the *x*, *y*, and *z* axes, (called *u*, *v* and *w*, respectively) should be added to the coordinates denoted by prime. By equating these two different representations, one may write:

$$\begin{Bmatrix} l_0\sin\left(\frac{\theta}{2}\right)\cos(\phi)+u \\ l_0\cos\left(\frac{\theta}{2}\right)\cos(\phi)+v \\ l_0\sin(\phi)+w \end{Bmatrix}=\begin{Bmatrix} l\sin\left(\frac{\theta}{2}-\delta\theta\right)\cos(\phi+\delta\phi) \\ l\cos\left(\frac{\theta}{2}-\delta\theta\right)\cos(\phi+\delta\phi) \\ l\sin(\phi+\delta\phi) \end{Bmatrix} \quad (8)$$

by expanding the trigonometric terms of Equation (8), a system of three equations is obtained as:

$$\begin{cases} l\left(\sin\left(\frac{\Theta}{2}\right)\cos(\phi)-\sin\left(\frac{\Theta}{2}\right)\sin(\phi)\delta\phi-\cos\left(\frac{\Theta}{2}\right)\cos(\phi)\delta\Theta\right)=l_0\sin\left(\frac{\Theta}{2}\right)\cos(\phi)+u \\ l\left(\cos\left(\frac{\Theta}{2}\right)\cos(\phi)-\cos\left(\frac{\Theta}{2}\right)\sin(\phi)\delta\phi+\sin\left(\frac{\Theta}{2}\right)\cos(\phi)\delta\Theta\right)=l_0\cos\left(\frac{\Theta}{2}\right)\cos(\phi)+v \\ l\left(\sin(\phi)+\cos(\phi)\delta\phi\right)=l_0\sin(\phi)w \end{cases} \quad (9)$$

Since $l-l_0=\delta l$ we have:

$$\begin{cases} \delta l\left(\sin\left(\frac{\Theta}{2}\right)\cos(\phi)-l_0\sin\left(\frac{\Theta}{2}\right)\sin(\phi)\delta\phi-l_0\cos\left(\frac{\Theta}{2}\right)\cos(\phi)\delta\Theta\right)=u \\ \delta l\left(\cos\left(\frac{\Theta}{2}\right)\cos(\phi)-l_0\cos\left(\frac{\Theta}{2}\right)\sin(\phi)\delta\phi+l_0\sin\left(\frac{\Theta}{2}\right)\cos(\phi)\delta\Theta\right)=v \\ \delta l\sin(\phi)+l_0\cos(\phi)\delta\phi=w \end{cases} \quad (10)$$

Therefore, from the system of equations appeared in Equation (10), variations of the displacement and rotation components may be determined as follows

$$\begin{cases} \delta\theta = \dfrac{sec\left(\phi\right)\left(-u\,cos\left(\dfrac{\theta}{2}\right)+v\,sin\left(\dfrac{\theta}{2}\right)\right)}{l_0} \\ \delta\phi = \dfrac{w\,cos\left(\phi\right)-sin\left(\phi\right)\left(u\,sin\left(\dfrac{\theta}{2}\right)+v\,cos\left(\dfrac{\theta}{2}\right)\right)}{l_0} \\ \delta l = \left(u\,sin\left(\dfrac{\theta}{2}\right)+v\,cos\left(\dfrac{\theta}{2}\right)\right)cos\left(\phi\right)+w\,sin\left(\phi\right) \end{cases} \quad (11)$$

The initial ϕ angle is zero and ɵ is equal to 120 or -120 degrees for the upper part (nodes number 1, 2, and 3) and lower part (nodes number 4, 5, and 6) of the hexagon. Inserting these values in the Equation (11), the following expressions can be obtained for the displacement increments:

$$\theta = 120°: \begin{cases} \delta\theta_1 = -\dfrac{u_2-\sqrt{3}v_2}{2l_0} \\ \delta\phi_{23} = \dfrac{w_3}{l_0} \\ \delta l_{23} = \dfrac{1}{2}\left(\sqrt{3}u_2+v_2\right) \end{cases} \quad (12a)$$

$$\theta = -120°: \begin{cases} \delta\theta_2 = -\dfrac{u_6+\sqrt{3}v_6}{2l_0} \\ \delta\phi_{46} = \dfrac{w_4}{l_0} \\ \delta l_{46} = \dfrac{1}{2}\left(v_6-\sqrt{3}u_6\right) \end{cases} \quad (12b)$$

By substituting Equation (12) into Equation (7), the potential energy can be determined.

2.2. The effective 2D Young's Modulus of the Nanosheet

In order to determine the effective Young's modulus, the total potential energy should be considered. The work of the external forces is:

$$E_{external} = -2F_{2x}u_2 - 2F_{6x}u_6 \quad (13)$$

and the total potential energy of the unit cell may be defined as:

$$E_T = E_{internal} - E_{external} \quad (14)$$

The first derivative of the total energy, E_T, with respect to the atomic displacements must be zero; since the total energy is minimal when the unit cell is in equilibrium:

$$\frac{\partial E_T}{\partial u_i} = 0,\ \frac{\partial E_T}{\partial v_i} = 0,\ \frac{\partial E_T}{\partial w_i} = 0,\ \therefore i = 2,6 \quad (15)$$

Using Equations (7) and (12-15), the following six linear equations are obtained:

$$\frac{1}{2}\left(4F_{2x}+k_r\left(3u_2+\sqrt{3}v_2\right)+\frac{3k_\theta\left(u_2-\sqrt{3}v_2\right)}{l_0^2}\right)=0$$
$$\Rightarrow 3u_2\left(k_r+\frac{k_\theta}{l_0^2}\right)+\sqrt{3}v_2\left(k_r-\frac{3k_\theta}{l_0^2}\right)=-4F_{2x} \quad (16a)$$

$$\frac{1}{2l_0^2}\left(k_r l_0^2\left(\sqrt{3}u_2+v_2\right)+k_\theta\left(9v_2-3\sqrt{3}u_2\right)\right)=0$$
$$\Rightarrow \sqrt{3}u_2\left(k_r-\frac{3k_\theta}{l_0^2}\right)+v_2\left(k_r+\frac{9k_\theta}{l_0^2}\right)=0 \quad (16b)$$

$$\frac{1}{2}\left(4F_{6x}+k_r\left(3u_6-\sqrt{3}v_6\right)+\frac{3k_\theta\left(u_6+\sqrt{3}v_6\right)}{l_0^2}\right)=0$$
$$\Rightarrow 3u_6\left(k_r+\frac{k_\theta}{l_0^2}\right)-\sqrt{3}v_6\left(k_r-\frac{3k_\theta}{l_0^2}\right)=-4F_{6x} \quad (16c)$$

$$\frac{1}{2l_0^2}\left(k_r l_0^2\left(v_6-\sqrt{3}u_6\right)+3k_\theta\left(\sqrt{3}u_6+3v_6\right)\right)=0$$
$$\Rightarrow \sqrt{3}u_6\left(k_r-\frac{3k_\theta}{l_0^2}\right)-v_6\left(k_r+\frac{9k_\theta}{l_0^2}\right)=0 \quad (16d)$$

$$\frac{2}{l_0^2}k_\tau w_2 = 0 \quad (16e)$$

$$\frac{2}{l_0^2}k_\tau w_6 = 0 \quad (16f)$$

v_2 and v_6 can be deduced from Equations (16b) and (16c) as functions of u_2 and u_6, respectively:

$$v_2 = \frac{\sqrt{3}u_2\left(3k_\theta - k_r l_0^2\right)}{k_r l_0^2 + 9k_\theta} \quad (17a)$$

$$v_6 = -\frac{\sqrt{3}u_6\left(3k_\theta - k_r l_0^2\right)}{k_r l_0^2 + 9k_\theta} \quad (17b)$$

Knowing that $F_x = F_{2x} + F_{6x}$ and $u_2 = u_6$, under a simple compression and combining Equations (16a) and (16c), and using Equation (17), yield:

$$F_x = -12u_2k_r\left(\frac{k_\theta}{k_r l_0^2+9k_\theta}+\frac{k_\theta}{k_r l_0^2+9k_\theta}\right)= -12u_2k_r\left(\frac{1}{\frac{k_r l_0^2}{k_\theta}+9}+\frac{1}{\frac{k_r l_0^2}{k_\theta}+9}\right) \quad (18)$$

Axial (*x*-direction) stress and strain of the unit cell can be determined as follows:

$$\sigma_x = \frac{F_x}{2l_0 t} \quad (19a)$$

$$\varepsilon_x = \frac{2u_2}{\sqrt{3}l_0} \quad (19b)$$

where t is the thickness of the sheet.

Young's modulus of the sheet is assumed to be equal to that of the unit cell. Based on Equations (18) and (19), the effective 2D Young's modulus of the sheet ($Y_s = \sigma_x t / \varepsilon_x$), can be evaluated as:

$$Y_s = 3\sqrt{3}k_r\left(\frac{1}{\frac{k_r l_0^2}{k_\theta}+9}+\frac{1}{\frac{k_r l_0^2}{k_\theta}+9}\right) \quad (20)$$

2.3. The buckling load

In order to determine the buckling load, description of the external load should be change:

$$E_{external} = M_3\times\delta\phi + M_4\times\delta\phi = \left(F_{2x}+F_{6x}\right)\times\left(l_0+\delta l\right)\times sin\left(\phi+\delta\phi\right)\times\delta\phi = \left(F_{2x}+F_{6x}\right)\delta\phi^2\left(l_0+\delta l\right) \quad (21)$$

Inserting Equation (21) into Equation (14) and using Equation (7), one has:

$$E = k_r\left[\left(\delta l_{23}\right)^2+\left(\delta l_{46}\right)^2\right]+3k_\theta\left[\left(\delta\theta_1\right)^2+\left(\delta\theta_2\right)^2\right]+ k_\tau\left[\left(\delta\phi_{23}\right)^2+\left(\delta\phi_{46}\right)^2\right]+2F_{2x}\delta\phi_{23}^2\left(l_0+\delta l_{23}\right)+ 2F_{6x}\delta\phi_{46}^2\left(l_0+\delta l_{46}\right) \quad (22)$$

Minimizing the total Energy with respect to w_3 and w_4 leads to the following equations:

$$\frac{2\left(3k_\tau+F_{2x}\left(2l_0+\sqrt{3}u_2+v_2\right)\right)w_3}{l_0^2}=0 \quad (23a)$$

$$\frac{2\left(3k_\tau+F_{6x}\left(2l_0-\sqrt{3}u_6+v_6\right)\right)w_4}{l_0^2}=0 \quad (23b)$$

Since in the buckling onset, the deformations are very small, products of the displacement components can be ignored. Therefore, Equation (23) may be linearize through omitting these products. On the other hand, in order to meet all the conditions, either w_3 (or w_4) or the parentheses multiplied by them in Equation (23) should be zero (in the linearized expressions). Indeed, since buckling appears as a lateral deflection (in *z*-direction) under the in-plane loads, other displacement terms may be set to zero in the linearization process; so that:

$$\begin{cases}\left(3k_\tau+F_{2x}\left(2l_0\right)\right)=0\\ \left(3k_\tau+F_{6x}\left(2l_0\right)\right)=0\end{cases} \quad (24)$$

Knowing that $F_x = F_{2x}+F_{6x}$, the total buckling load becomes:

$$6k_\tau+F_x\left(2l_0\right)=0\Rightarrow F_x=-\frac{3k_\tau}{l_0} \quad (25)$$

This would be the necessary load for the buckling of the nanosheet structure.

3. Verifications and numerical results

3.1. Verification of the presented formulations

Results of Equation (25) are verified based on the traditional results of a much simpler configuration, i.e., result of the proposed, expression for the buckling force would be compared with result of a well-known buckling problem.

3.1.1. Verification of Proposed expression for the effective Young's Modulus

In order to verify the proposed closed-form solutions, Equation (20) that is proposed for the effective Young's modulus is verified first through comparing it with the solution given in Reference [32] which gave the same formula through another complicated geometrical approach. The relevant expression of Reference [32] for the 2D Young's modulus is:

$$Y_s = 3\sqrt{3}K\left[\frac{1}{\frac{Kl_0^2}{C_1}+9}+\frac{1}{\frac{Kl_0^2}{C_2}+9}\right] \quad (26)$$

where *K*, C_1 and C_2 denote force constants associated with bond stretching and bond angles increments, respectively. Although Equation (26) has been derived based on the second Newton's law rather than the energy approach, it is in a good agreement with Equation (20). Li [32] has verified his formula numerically by substituting adequate force constants for different nanosheets and comparing the results with about to 30 other references.

3.1.2. Verification of the proposed solution for the buckling load

The very simple structure shown in Figure 5 which is composed of two rigid members that can carry only axial forces and torsional moments at the mutual joint (with a local torsional stiffness *k*) is adopted to verify results of Equation (25). At the buckling onset, the joint experiences an angular deformation, i.e., ϕ (in the *x*-*z* plane).

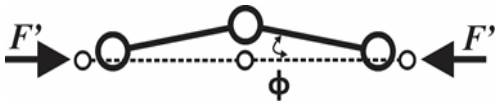

Fig. 5. The considered two-member structure (with a localized torsional stiffness) for verification of the predicted buckling load

The static buckling state requires that the applied load maintains the resulting lateral deflection in the equilibrium state, i.e.,

$$M = Fl\sin\phi = k_\tau\phi \tag{27}$$

where *l* is the length of the members. In the buckling onset, the displacements may be regarded to be very small; so that sin ϕ in Equation (27) may be replaced by ϕ. Therefore:

$$F = \frac{k_\tau}{2l} \tag{28}$$

This result can exactly be deduced from Equation (25), for the present very special configuration. Indeed, to this end, the effective length and torsional stiffness of the unit cell (in the x-z plane) that are originally defined in a plane that makes an angle of 30 degrees with the *x*-*z* plane, should be determined in the *x*-z plane. On the other hand, noting that the original ϕ angle of the unit cell has been defined in the $\theta = \pi/3$ plane ($k_\tau = \left(\frac{M}{\phi}\right)_{\theta=\pi/3}$) and not in the x-z plane, the following relations may be used to relate the spatial quantities [33]:

$$(k)_{eq}\big|_{x-z\ plane} / l_{eq} = \left[k_\tau \cos\left(\frac{\pi}{6}\right)\tan^2\left(\frac{\pi}{3}\right)\right] / l_0\cos\left(\frac{\pi}{6}\right) = \frac{3k_\tau}{l_0}, \tag{29}$$

Substituting the effective quantities appeared in Equation (29) into Equation (30) and using Equation (24), the following buckling load may be predicted:

$$F = 2F_{2x} = 2F_{6x} = 2\left[\frac{(k)_{eq}}{2l_{eq}}\right] = \frac{3k_\tau}{l_0} \tag{30}$$

Equation (30) is identical to Equation (25).

3.2. Numerical results

In this section, new numerical results are presented for different nanosheets. The required material properties and constants are gathered from various references. For graphene, k_τ and l_0 are extracted from [29]. Parameters of the boron nitride are obtained from [34] and [35-37] and properties of the silicon carbide nanosheet, are taken from [25] and [38]. These parameters are listed in Table 1 along with the local buckling loads determined based on Equation (25).

Therefore, the local buckling of boron nitride nanosheet is about two times that of the grapheme which is in turn, about one half of that of the silicon carbide nanosheet. The proposed formulations, both for 2D Young modulus and local buckling load, are applicable to all kinds of nanoplates with hexagonal structures. By substituting the corresponding force field parameters of the quantum mechanics which may predict the interactions of the nanosheet's constituents, results would be easily obtained by present formulations.

Although unique stiffness parameters have not been reported in literature, but to show the applicability of proposed formulations, some typical force field parameters which have been derived based on various approaches are given in Table 2, for the grapheme, boron nitride, and silicon carbide nanosheets.

Table 1. Local buckling loads of different types of nanosheets

Type of the nanosheet	k_τ (nN nm rad^{-2})	L_0(nm)	$F_{buckling}$(nN)
Graphene	0.279	0.1421	5.8902
Boron nitride	0.6255	0.145	12.941
Silicon carbide	1.505	0.179	25.223

Table 2. Stiffness parameters of the grapheme, boron nitride, and silicon carbide nanosheets

Nanosheet	Force field	k_r [N nm^{-1}]	k_θ [N nm rad^{-2}]	k_τ [N nm rad^{-2}]
Graphene	AMBER [29]	6.52×10^{-7}	8.76×10^{-10}	2.78×10^{-10}
	Morse [29]	8.74×10^{-7}	9.00×10^{-10}	2.78×10^{-10}
Boron nitride	DREIDING [49]	4.8731343×10^{-7}	6.97619×10^{-10}	6.255×10^{-10}
	UFF [30]	6.757×10^{-7}	1.74614×10^{-9}	6.255×10^{-10}
Silicon carbide	SiC [25]	4.17156×10^{-7}	8.42×10^{-10}	1.505×10^{-9}

Table 3. A comparison between the predicted 2D Young Moduli and those predicted by other references, for the three types of the nanosheet

Nanosheet	Reference	Y_s N/m
Graphene	*Present study, based on AMBER force field parameters*	277.314
	Present study, based on Morse force field parameters	320.874
	Proposed formula with harmonic force field parameters by Le [32]	300
	Scarpa et. Al [29] based on AMBER potential	260
	Scarpa et. Al [29] based on Morse potential	327
	Experiment by Lee et al [34]	340
	DFT by Sahin et al. [40]	335
	Berinskii and Krivtsov [41] based on REBO potential	243
	Berinskii and Krivtsov [41] based on Tersoff-Brenner potential	236
Boron Nitride	*Present study, based on DREIDING force field parameters*	213.803
	Present study, based on UFF force field parameters	322.653
	Proposed formula with harmonic force field parameters by Le [32]	332
	Experiment by Song et al. [42]	223±16
	Ab initio by Kudin et al. [43]	236
	Oh [44] based on Tersoff-Brenner potential	322
	Molecular Dynamics by Mortazavi and Reymond[35]	280
	Terso-like potential [46]	322
	UFF potential [47]	328
	Cohesive energy [48]	
Silicon Carbide	*Present study*	174.285
	Proposed formula with harmonic force field parameters by Le [32]	162
	Molecular dynamics simulation based on Tersoff-like potential [49]	173.4
	DFT by Sahin et al. [40]	166

The computed effective values of the 2D Young's modulus, based on Equation (19), are presented in Table 3. It is evident that various approaches of determination of the stiffness parameters have led to some discrepancies among the results but results of each category of the stiffness parameters are almost in a good agreement. Along with other results, results of reference [32] are also presented. The differences between the results are ignorable and the discrepancies are due to using different force field parameters. In reference [32], harmonic force field parameters were used and modified for each nanosheet, whereas, in the present study, defferent force fields are used for each nanosheet depending on its constituents' characteristics.

Due to the fact that the authors have intended to develop formulations for both the 2D Young's modulus and the buckling load based on identical models, all of the relations are given in general forms, taking into account all the variables which may potentially affect the results. However, regarding to Equations (19) and (25), torsional stiffness has a negligible effect on effective 2D Young's modulus, in contrast to the bending and longitudinal stiffnesses which are absent from the final local buckling load formulation. It can be concluded that although it may seem that accounting for the torsional stiffness may affect all the elastic properties; the results have proven that the 2D properties are independent of the torsional stiffness. Therefore, if two

different materials with identical longitudinal and bending stiffnesses but different torsional stiffness are adopted, both would show the same effective in-plane elastic properties.

Buckling load has a linear relationship with the torsional stiffness, i.e. higher values of torsional stiffness lead to higher buckling loads. However, this issue does not hold for the 2D Young's modulus, since its expression is much more complicated than that of the buckling load. Therefore, derivation of a logical relationship between the bending and longitudinal stiffnesses and the calculated 2D Young's modulus may be a complicated task.

4. Conclusions

In the present study, a three-dimensional space-frame-like geometrical model is employed to propose closed-form solutions for both the local buckling load (cell buckling) and effective 2D Young's modulus of different nanosheets. In this model the stiffnesses of the atomic bonds are considered based on various molecular dynamics approaches. The Energy method is used in derivation of the closed-form expressions of the local buckling load and the effective 2D Young's modulus. The 2D Young's modulus expression is verified by the available closed-form relations available in literature. Verification of results of the buckling load is accomplished in two different approaches. First, a simple structure with a known traditional solution is considered. Then, using values available in literature for the bonds stiffness parameters, a comparison is made for different types of nanosheets (graphene, boron nitride, and silicon carbide) and a good agreement is noticed with the results available in literature.

References

[1].Oberlin A., Endo M., Koyama T., 1976, Filamentous Growth of Carbon through Benzene Decomposition, *Journal of Crystal Growth* **32**(3): 335-349.

[2].Iljima S., 1991, Helical microtubules of graphitic carbon, *Letters to Nature* **354**: 56-58.

[3].Novoselov K.S., Geim A.K., Morozov S.V., Jiang D., Zhang Y., Dubonos S.V., Grigorieva I.V., Firsov A.A., 2004, Electric Field Effect in Atomically Thin Carbon Films, *Science* **306**: 666-669.

[4].Corso M., Auwarter W., Muntwiler M., Tamai A., Greber T., Osterwalder J., 2004, Boron Nitride Nanomesh, *Science* **303**: 217-220.

[5].Castellanos-Gomez A., Poot M., Steele G.A., van der Zant H.S.J., Agraït N., Rubio-Bollinger G., 2012, Elastic Properties of Freely Suspended MoS2 Nanosheets, *Advaced Materials* **24**(6): 772–775.

[6].Xu M., Liang T., Shi M., Chen H., 2013, Graphene-Like Two-Dimensional Materials, *Chemical Reviews* **113**(5): 3766–3798.

[7].Wang C.M., Zhang Y.Y., Ramesh S.S., Kitipornchai S., 2006, Buckling analysis of micro- and nano-rods/tubes based on nonlocal Timoshenko beam theory, *Jouranl of Physics D: Applied Physics* **39**: 3904–3909,.

[8].Wanga Q., Duan W.H., Liew K.M., He X.Q., 2007, Inelastic buckling of carbon nanotubes, *Applied Physics Letters* **90**: 033110.

[9].Sudak L.J., 2003, Column buckling of multiwalled carbon nanotubes using nonlocal continuum mechanics, *Journal of Applied Physics* **94**(11): 7281-7287.

[10]. Wang Q., Wang C.M., 2007, The constitutive relation and small scale parameter of nonlocal continuum mechanics for modelling carbon nanotubes, *Nanotechnology* **18**: 075702.

[11]. Lu P., Lee H.P., Lu C., Zhang P.Q., 2007, Application of nonlocal beam models for carbon nanotubes, *International Journal of Solids and Structures* **44**: 5289–5300.

[12]. Shi M.X., Li Q.M., Liu B., Feng X.Q., Huang Y., 2009, Atomic-scale finite element analysis of vibration mode transformation in carbon nanorings and single-walled carbon nanotubes, *International Journal of Solids and Structures* **46**: 4342–4360.

[13]. Moosavi H., Mohammadi M., Farajpour A., Shahidi S.H., 2011, Vibration analysis of nanorings using nonlocal continuum mechanics and shear deformable ring theory, *Physica E* **44**: 135–140.

[14]. Danesh M., Farajpour A., Mohammadi M., 2012, Axial vibration analysis of a tapered nanorod based on nonlocal elasticity theory and differential quadrature method, *Mechanics Research Communications* **39**: 23– 27.

[15]. Aydogdu M., 2012, Axial vibration analysis of nanorods (carbon nanotubes) embedded in an elastic medium using nonlocal elasticity, *Mechanics Research Communications* **43**: 34–40.

[16]. Arash B., Wang Q., 2012, A review on the application of nonlocal elastic models in modeling of carbon nanotubes and graphenes, *Computational Materials Science* **51**: 303–313.

[17]. Pradhan S.C., 2009, Buckling of single layer graphene sheet based on nonlocal elasticity and

higher order shear deformation theory, *Physics Letters A* **373**: 4182–4188.

[18]. Narendar S., 2011, Buckling analysis of micro-/nano-scale plates based on two-variable refined plate theory incorporating nonlocal scale effects, *Composite Structures* **93**: 3093–3103.

[19]. Samaeia A.T., Abbasion S., Mirsayar M.M., 2011, Buckling analysis of a single-layer graphene sheet embedded in an elastic medium based on nonlocal Mindlin plate theory, *Mechanics Research Communications* **38**: 481–485.

[20]. Farajpour A., Mohammadi M., Shahidi A.R., Mahzoon M., 2011, Axisymmetric buckling of the circular graphene sheets with the nonlocal continuum plate model, *Physica E* **43**: 1820–1825.

[21]. Farajpour A., Shahidi A.R., Mohammadi M., Mahzoon M., 2012, Buckling of orthotropic micro/nanoscale plates under linearly varying in-plane load via nonlocal continuum mechanics, *Composite Structures* **94**: 1605–1615.

[22]. Narendar S., Gopalakrishnan S., 2012, Scale effects on buckling analysis of orthotropic nanoplates based on nonlocal two-variable refined plate theory, *Acta Mechanica* **223**: 395–413.

[23]. Ansari R., Rouhi S., Aryayi M., Mirnezhad M., 2012, On the buckling behavior of single-walled silicon carbide nanotubes, *Scientia Iranica* **19**(6): 1984–1990.

[24]. Tourki Samaei A., Hosseini Hashemi Sh., 2012, Buckling analysis of graphene nanosheets based on nonlocal elasticity theory, *International Journal of Nano Dimension* **2**(4): 227-232.

[25]. Ansari R., Rouhi S., Mirnezhad M., Aryayi M., 2013, Stability characteristics of single-layered silicon carbide nanosheets under uniaxial compression, *Physica E* **53**: 22–28.

[26]. Bedroud M., Hosseini-Hashemi S., Nazemnezhad R., 2013, Buckling of circular/annular Mindlin nanoplates via nonlocal elasticity, *Acta Mech* **224**(11): 2663-2676.

[27]. Sobhy M., 2015, Levy-type solution for bending of single-layered graphene sheets in thermal environment using the two-variable plate theory, *International Journal of Mechanical Sciences* **90**: 171–178.

[28]. Hosseini-Hashemi S., Kermajani M., Nazemnezhad R., 2015, An analytical study on the buckling and free vibration of rectangular nanoplates using nonlocal third-order shear deformation plate theory, *European Journal of Mechanics A/Solids* **51**: 29-43.

[29]. Scarpa F., Adhikari S., Gil A.J., Remillat C., 2010, The bending of single layer graphene sheets: the lattice versus continuum approach, *Nanotechnology* **21**: 125702 (9pages).

[30]. Casewit C. J., Colwell K.S., Rappe A.K., 1992, Application of Universal Force Field to Organic Molecules, *Journal of American Chemical Society* **114**(25): 10035-10046.

[31]. Song L., Ci L., Lu H., Sorokin P.B., Jin Ch., Ni J., Kvashnin A.G., Kvashnin D.G., Lou J., Yakobson B.I., Ajayan P.M., 2010, Large Scale Growth and Characterization of Atomic Hexagonal Boron Nitride Layers, *Nano Letters* **10**: 3209-3215.

[32]. Le M.Q., 2014, Prediction of Young's modulus of hexagonal monolayer sheets based on molecular mechanics, *International Journal of Mechanics and Materials in Design*, DOI: 10.1007/s10999-014-9271-0.

[33]. Fitzpatrick R., 2012, *An Introduction to Celestial Mechanics*, Cambridge University Press.

[34]. Lee C., Wei X., Kysar J.W., Hone J., 2008, Measurement of the elastic properties and intrinsic strength of monolayer grapheme, *Science* **321**: 385-388.

[35]. Mortazavi B., Remond Y., 2012, Investigation of tensile response and thermal conductivity of boron-nitride nanosheets using molecular dynamics simulation, *Physica E* **44**: 1846-1852.

[36]. Panchal M. B., Upadhyay S. H., 2014, Boron nitride nanotube-based biosensor for acetone detection: molecular mechanics-based simulation, *Molecular Simulation* **40**(13): 1035-1042.

[37]. Akdim B., Kim S.N., Naik R.R., Maruyama B., Pender M.J., Pachter R., 2009, Understanding effects of molecular adsorption at a single-wall boron nitride nanotube interface from density functional theory calculations, *Nanotechnology* **20**: 355705.

[38]. Erhart P., Albe K., 2005, Analytical potential for atomistic simulations of silicon, carbon, and silicon carbide, *Physical Review B* **71**: 035211.

[39]. Chowdhurry R., Wang C.Y., Adhikari S., Scarpa F., 2010, Vibration and symmetry-breaking of boron nitride nanotubes, *Nanotechnology* **21**: 365702.

[40]. Sahin H., Cahangirov S., Topsakal M., Bekaroglu E., Akturk E., Senger R.T., Ciraci S., 2009, Monolayer honeycomb structures of group-IV elements and III-V binary compounds: first-principles calculations, *Physical Review B* **80**: 155453.

[41]. Berinskii I.E., Krivtsov A.M., 2010, On using many-particle interatomic potentials to compute elastic properties of graphene and diamond, *Mechanics of Solids* **45**: 815.

[42]. Song L., Ci L., Lu H., Sorokin P.B., Jin Ch., Ni J., Kvashnin A.G., Kvashnin D.G., Lou J., Yakobson B.I., Ajayan P.M., 2010, Large Scale Growth and Characterization of Atomic Hexagonal Boron Nitride Layers, *Nano Letters* **10**: 3209-3215.

[43]. Kudin K.N., Scuseria G.E., Yakobson B.I., 2001, C2F, BN, and C nanoshell elasticity from ab initio computations, *Physical Review B* **64**: 235406.

[44]. Oh E.S., 2010, Elastic properties of boron-nitride nanotubes through the continuum lattice approach, *Materials Letters* **64**: 859–862.

[45]. Oh E.S., 2011, Elastic Properties of Various Boron-Nitride Structures, Metals and Materials International **17**(1): 21-27.

[46]. Boldrin L., Scarpa F., Chowdhury R., Adhikari S., 2011, Effective mechanical properties of hexagonal boron nitride nanosheets, *Nanotechnology* **22**: 505702.

[47]. Bosak A., Serrano J., Krisch M., Watanabe K., Taniguchi T., Kanda H., 2006, Elasticity of hexagonal boron nitride: Inelastic x-ray scattering measurements, *Physical Review B* **73**: 041402.

[48]. Le M. Q., 2014, Atomistic study on the tensile properties of hexagonal AlN, BN, GaN, InN and SiC sheets, *Journal of Computational and Theoretical Nanoscience* **11**: 1458–1464.

[49]. Li C., Chou T.W., 2003, A structural mechanics approach for the analysis of carbon nanotubes, *International Journal of Solids and Structures* **40**: 2487-2499.

[50]. Mayo S.L., Olafson B.D., Goddard W.A., 1990, DREIDING: A Generic Force Field for Molecular Simulations, *Journal Physical Chemistry* **94**(26): 8897-8909.